Eur. Phys. J. D **45**, 301–308 (2007)
DOI: 10.1140/epjd/e2007-00283-5

THE EUROPEAN PHYSICAL JOURNAL D

Combined experimental and theoretical study of small aluminum oxygen clusters*

S. Neukermans[1], N. Veldeman[1], E. Janssens[1], P. Lievens[1,a], Z. Chen[2], and P.v.R. Schleyer[2]

[1] Laboratorium voor Vaste-Stoffysica en Magnetisme & INPAC, Institute for Nanoscale Physics and Chemistry, Katholieke Universiteit Leuven, 3001 Leuven, Belgium
[2] Center for Computational Chemistry, Department of Chemistry, University of Georgia, Athens, 30602 Georgia, USA

Received 10 May 2007 / Received in final form 18 June 2007
Published online 5 October 2007 –

Abstract. We report a combined experimental and computational investigation of small Al_nO_m species ($n \leq 20$, $m \leq 12$), produced in a laser vaporization cluster source. The oxygen content in the clusters was tuned by varying the oxygen concentration in the carrier gas. Ionization energies are bracketed using different ionizing photon energies in the energy range between 5.37 and 7.89 eV. Among the singly doped Al_nO species, Al_3O and $Al_{15}O$ are found to have relatively low ionization energies, which can be related to the magic character of the corresponding cations. Peculiarly low ionization energies also are observed for specific oxygen rich species ($m > 1$), suggesting the formation of ionically bound subunits. The structures and ionization energies of singly doped $Al_nO^{0,+}$ ($n = 1-7$) clusters were determined using density functional theory (B3LYP/6-311+G(d)).

PACS. 36.40.Cg Electronic and magnetic properties of clusters – 36.40.Mr Spectroscopy and geometrical structure of clusters – 31.15.Ew Density-functional theory

1 Introduction

Aluminum oxide is employed in material science in numerous protective coatings, ceramic materials, minerals, and oxide surfaces that serve as catalysts or their substrates. Although size significantly affects the characteristics of bulk aluminum oxide, small clusters are useful models to understand its structure and bonding as well as the role of defect sites on surfaces or the physics and chemistry of the oxide surfaces in general, as their small size allows for accurate computational studies [1–17]. Oxygen doped aluminum clusters also are possible "superatom" candidates having tailored chemical properties [18].

Pure aluminum clusters have well been characterized by numerous experimental and high level theoretical studies [19–27]. Aluminum, the smallest metallic trivalent element, offers the possibility to alter the number of delocalized electrons in clusters compared to mono- and divalent elements. Like the clusters of the heavier trivalent main group metals such as In and Tl [28,29], optimum delocalization of the three ($3s^23p^1$) valence electrons per Al atom over the entire cluster volume gives rise to "magic numbers" in the size dependent properties of aluminum clusters, that correspond to electronic shell closures [19,20]. Not only the electronic structure, but also the close-packed geometry of aluminum clusters is important [21]. For example, icosahedral (I_h) structures are found to be either the most stable or low-lying isomers of Al_{13} as well as its ions [23,25,27,30,31]. From Al_{55} on a transition to fcc cuboctahedral (O_h) lattice structures occurs [22–24].

Increasing oxygen content in doped aluminum clusters, structural or geometric effects will govern the observed size-dependent properties (ionization energy, electron affinity, stability) because of an increased number of ionic bonds. Related studies on partly oxidized metal clusters showed segregation between ionically bound and metallic units [32–40], but despite of this, shell structures still can be observed. In a threshold photoionization study of (monovalent) cesium oxide clusters, peculiarly high ionization energy values were found for $Cs_{z+2n}O_n$ species with $z = 8, 18, 34, 58, 92, \ldots$ sizes that correspond to magic numbers resulting from a simple spherical shell model [35]. Most probably, segregation occurs between an ionically bound $Cs_{2n}O_n$ unit and a shell of z surrounding Cs atoms, which leads to the unexpected spherically symmetric potential well in which z delocalized valence electrons are moving. In oxygen or carbon doped lithium clusters electronic shell closings could be identified in the size dependent pattern of the ionization energies [32–34,41]. A unimolecular evaporation study of lithium rich $Li_nH_m^+$ cluster ions indicates a clear separation between a metallic Li_{n-m}^+ part and an insulating $(LiH)_m$ part [38]. In the case of (divalent) barium oxide clusters there is evidence for segregation between a $(BaO)_3$ or $(BaO)_4$ core and a metallic Ba_n shell [39,40].

* Supplementary Online Materials are available in electronic form at `www.epj.org`

[a] e-mail: `peter.lievens@fys.kuleuven.be`

In this paper, we report on the production, stability and ionization energy of oxygen doped aluminum clusters. These are produced in a laser vaporization cluster source. Different oxygen concentrations in the carrier gas were used to tune the amount of oxygen in the clusters. The ionization energy of a large number of Al_nO_m clusters ($n \leq 20$, $m \leq 12$) is bracketed using different ionizing photon energies in the energy range between 5.37 eV and 7.89 eV. The small singly doped Al_nO clusters ($n = 1-7$) are investigated in more detail by performing density functional theory (DFT) calculations and by comparing with calculated In_nO species studied earlier [42]. We focus on Al_7O and $Al_{15}O$, in order to explain their relatively low ionization energy values observed.

2 Production of binary Al_nO_m clusters

The cluster beam setup and the laser vaporization source have been described in detail [43]. The metal vapor formed through laser ablation of a rectangular aluminum target in the cluster source is entrained in a pulsed flow of He carrier gas. After the initial cluster aggregation, the mixture of atoms, clusters, and inert gas is expanded into a vacuum. This expansion reduces the temperature and stops further cluster formation. The central part of the cluster-gas beam, selected by a skimmer, enters the extraction region of a reflectron time-of-flight (RTOF) mass spectrometer, where laser light can ionize neutral clusters. The resulting cationic clusters are accelerated into the spectrometer and registered mass selectively by a dual microchannel plate detector. Our pure metal clusters were produced using a pure metallic target and 99.9999% He carrier gas combined with an effective gas filter. Only a limited number of oxygen doped species were formed under these conditions. Clusters with higher oxygen contents were obtained by introducing oxygen into the carrier gas. This technique already has been used, e.g., for the study of oxygen doped cesium [35] and barium [39,40] clusters. We probed different He carrier gas mixtures, containing 0 to 10% O_2, to tune the degree of oxygen doping in the aluminum clusters. Besides the expected increase in oxygen/aluminum ratio in the produced Al_nO_m species (representative mass spectra can be found in the Supplementary Online Material), the mass abundance spectra for the most oxygen rich carrier gases feature peculiar stability patterns (Fig. 1). Using the 0.2% O_2 in 99.8% He mixture (Fig. 1a), the most abundant species are built up of (AlO) units, i.e. the aluminum atoms are in the +II oxidation state. The following sequences are observed: $[(AlO)_nAl_3]^+$, $[(AlO)_nAl_2]^+$, $[(AlO)_nAl]^+$, showing a clear odd-even behavior with maxima for n even, odd, and even respectively, and $(AlO)_n^+$, $[(AlO)_nO]^+$, showing no clear odd-even pattern. Using the even more oxygen rich carrier gas containing 90% He (99.9999% purity) and 10% O_2 (99.9995% purity), the most abundant species are build up of (Al_2O_3) and (AlO) units (Fig. 1b), i.e. the aluminum atoms are in +III and +II oxidation states, respectively. Analysis of the mass spectrum indicates that the main peaks correspond to $[(Al_2O_3)_m(AlO)_n]^+$ sequences

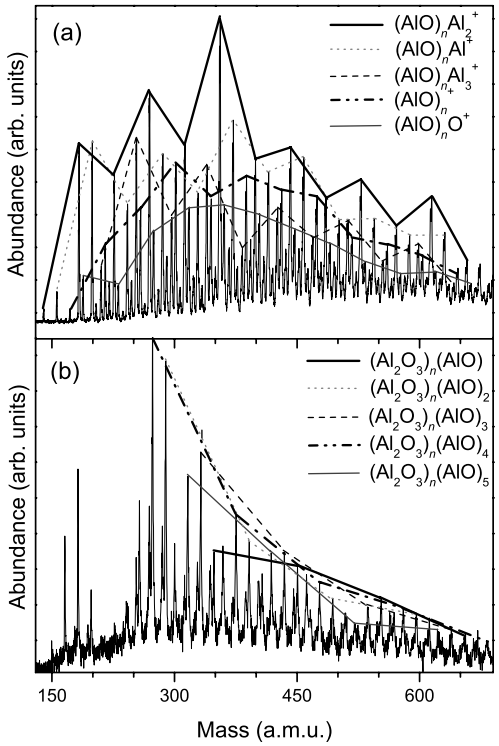

Fig. 1. (a) Mass abundance spectrum of cationic oxygen doped aluminum clusters produced using a mixture of 0.2% O_2 in 99.8% He as a carrier gas. The following series are connected by lines: $[(AlO)_nAl_3]^+$ ($n \geq 2$), $[(AlO)_nAl_2]^+$ ($n \geq 3$), $[(AlO)_nAl]^+$ ($n \geq 3$), showing a clear odd-even behavior with maxima for n even, odd, and even, respectively, and $(AlO)_n^+$ ($n \geq 4$), $[(AlO)_nO]^+$ ($n \geq 4$), showing no clear odd-even pattern. (b) Mass abundance spectrum of cationic oxygen doped aluminum clusters produced using a mixture of 10% O_2 in 90% He as a carrier gas. The peaks corresponding to $[(Al_2O_3)_m(AlO)_n]^+$ ($m > 1$; $n = 1-5$) are connected by lines. No odd-even pattern is present.

($m > 1$; $n = 1-6$) (Fig. 1b). The latter sequences do not show any odd-even variation in their abundance.

The formation of $[(MO)_nM]^+$ species previously has been observed for gallium oxide cations in a stability and reactivity study of group 13 metal oxides produced from sputtering and laser vaporization of pressed metal oxide powders [9]. In the same study, for Al and In, the principal ion series observed correspond to $[(M_2O_3)_nMO]^+$ and $[(M_2O_3)_nM_2O_2]^+$. The latter are similar to the series that we observe using our carrier gas mixture containing 10% O_2. AlO-$(Al_2O_3)_n$ species, produced from laser ablation of an aluminum target in a 1–10% O_2 in argon mixture, have been reported in experimental infrared REMPI studies [16,17].

3 Ionization energy bracketing of Al_nO_m ($1 \leq n \leq 20$, $1 \leq m \leq 12$)

The ionization energies (IE) of Al_nO_m ($1 \leq n \leq 20$, $1 \leq m \leq 12$) clusters were determined from a series of

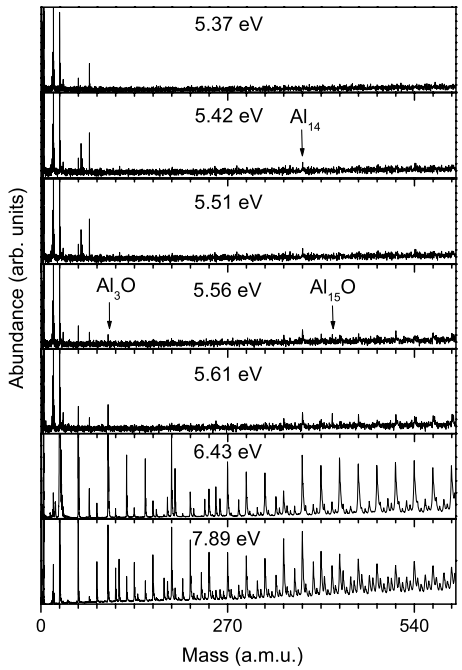

Fig. 2. Mass abundance spectra of Al_nO_m clusters ($n \leq 20$, $m \leq 4$) at different ionizing photon energies. Low IE values are observed for the Al_3O and $Al_{15}O$ "magic clusters". The unlabeled species that appear in the 5.56 eV and 5.61 eV spectra correspond to bare Al_n clusters.

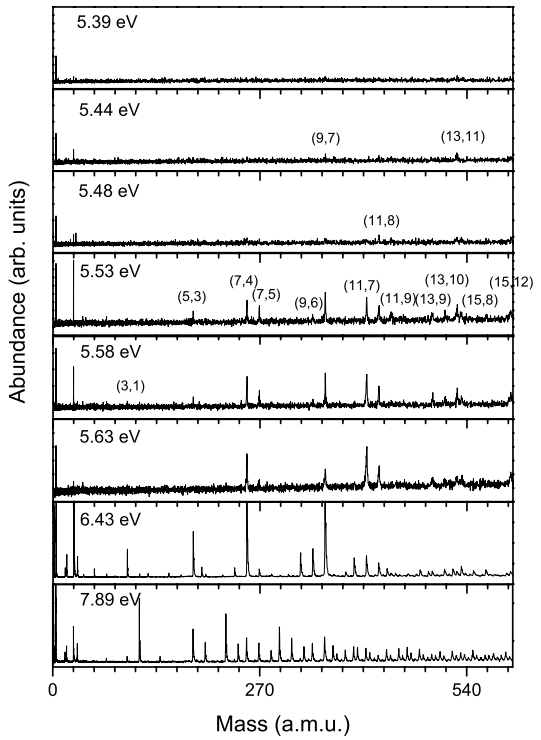

Fig. 3. Mass abundance spectra of Al_nO_m clusters ($n \leq 20$, $3 \leq m \leq 12$) at different photon energies. Al_nO_m clusters with low IE's are identified by (n, m) in the spectra where the ionization onset is observed.

mass abundance spectra. These were measured at different photon energies ranging from 5.37 eV to 7.89 eV, using a tunable optical parametric oscillator laser system covering a wavelength range down to 220 nm (laser photon energy of about 5.63 eV) as well as two excimer lasers having 193 nm (6.43 eV) and 157 nm (7.89 eV) fixed wavelengths. The IE values correspond to the onset of ionization. In the wavelength range above 220 nm (5.63 eV) mass spectra were recorded in 1 nm steps up to 231 nm (5.37 eV). The IE uncertainty is estimated to be of the order of 0.1 eV. If no signal is detected for a cluster in the mass spectrum using the highest tunable ionizing photon energy (5.63 eV), but a clear signal is observed in the fixed 6.43 eV spectrum, the IE lies between 5.63 and 6.43 eV. If only the fixed 7.89 eV spectrum reveals a clear signal, the IE lies between 6.43 and 7.89 eV. Figure 2 shows mass abundance spectra of oxygen doped aluminum clusters produced using He (99.995% purity) carrier gas after low fluence laser ionization at different photon energies in the 5.37 eV to 7.89 eV range. These measurements bracket the ionization energies of the Al_nO_m clusters ($n \leq 20$, $m \leq 4$). The same measurement performed for species produced using He (99.999% purity) carrier gas give identical results, but are limited to fewer Al_nO_m clusters ($n \leq 20$, $m \leq 2$). Ionization energies of the more oxygen-rich species (Al_nO_m clusters with $n \leq 16$ and $m \leq 12$, and $1 \leq n - m \leq 7$) are bracketed by measurements on oxygen doped aluminum clusters produced using an 0.2% O_2 in 99.8% He mixture as a carrier gas. Selected mass spectra taken at different ionization photon energies are shown in Figure 3.

Table 1 lists the ionization energies of the smaller singly oxygen-doped Al_nO ($n = 1{-}10, 15$) clusters and the more oxygen rich species with IE's below the highest available tunable photon energy (see the Supplementary Online Material for the complete data set). The "$\sim$6.43 eV" notation indicates the observation of a tiny signal (onset of ionization) at that energy along with a prominent signal in the 7.89 eV mass spectrum. Al_3O and $Al_{15}O$ have low IE's among the singly doped Al_nO species. The Al_7O IE also is smaller than the values of the neighboring sizes.

4 Discussion and comparison with DFT computations

Three sets of species, small singly doped ($n = 1{-}6$; $m = 1$), larger singly doped ($n = 7, 15$; $m = 1$) and multiply doped ($m > 1$), are discussed in separate sections. The computed DFT Al_nO ($n = 1{-}7$) clusters are compared with the In_nO structures [42] and with a recent study on Al_nO by Yang et al. [7]. Experimental and calculated ionization energy values of Al_nO clusters are compared. Computationally, we distinguish between the adiabatic ionization energy (aIE) and the vertical ionization energy (vIE) of the clusters. The aIE corresponds to the energy difference of the neutral and the ionized clusters, both in their relaxed ground states. The vIE is the energy difference between the neutral ground state and the

Table 1. Ionization energies (in eV) of selected Al_nO_m clusters. Uncertainties are estimated to be 0.10 eV (see text) when ranges are not given. All other Al_nO_m species probed have ionization energies above 5.63 eV. The full set of data is given in the Supplementary Online Material.

	IE (eV)		IE (eV)
AlO	>7.89	Al_5O_3	5.50
Al_2O	>7.89	Al_4O_7	5.50
Al_3O	5.55	Al_7O_5	5.50
Al_4O	5.63−6.43	Al_9O_6	5.55
Al_5O	5.63−6.43	Al_9O_7	5.45
Al_6O	∼6.43	$Al_{11}O_6$	5.55
Al_7O	5.63−6.43	$Al_{11}O_7$	5.50
Al_8O	6.43−7.89	$Al_{11}O_8$	5.50
Al_9O	5.63−6.43	$Al_{11}O_9$	5.50
$Al_{10}O$	5.63−6.43	$Al_{13}O_9$	5.50
$Al_{15}O$	5.55	$Al_{13}O_{10}$	5.50
		$Al_{13}O_{11}$	5.45
		$Al_{15}O_8$	5.50
		$Al_{15}O_{12}$	5.50

cation having the same geometry as the neutral. Geometry optimization computations for larger species were not performed. The origin of the relatively low ionization energy values measured for Al_7O and $Al_{15}O$ is discussed in more detail. Finally, the peculiarly low ionization energies observed for certain oxygen rich species ($m > 1$) are discussed.

4.1 Al_nO clusters (n = 1−6)

The geometries of the smallest Al_nO ($n = 1$−6) species were optimized at the B3LYP/6-311+G(d) DFT level using the Gaussian 03 program [44–47]. Most of the resulting minima, shown in Figures 4–6, are similar to the In_nO structures discussed in reference [42]. The exceptions (discussed below) are notable.

AlO has a doublet (**1**) and AlO^+ a triplet ground state (**2**). The Al−O bond lengths are 1.645 Å (AlO) and 1.768 Å (AlO^+). The AlO aIE and vIE are 9.87 eV and 10.07 eV, respectively. Both Al_2O (**4**) and Al_2O^+ (**5**) favor linear $D_{\infty h}$ geometries. The small difference in their Al−O bond lengths (1.732 Å and 1.723 Å, respectively) explains the nearly identical aIE (7.96 eV) and vIE (7.97 eV) values of Al_2O.

Al_3O and Al_4O already have been described extensively [2,3,5–7]. Our Al_3O computations gave a T-shaped C_{2v} minimum (**6**); the Y-shaped alternative (**7**) (0.09 eV higher in energy) is a transition structure for the degenerate interconversion of the T-forms. These findings contradict the earliest computations [3] but are in agreement with more recent results [5–7]. The two Al−O bond lengths in **6**, 1.833 Å and 1.989 Å, differ considerably. Like In_3O^+ [42], the Al_3O^+ cation (**8**) has a fully symmetric D_{3h} geometry with a closed electronic shell structure ($r_{Al–O} = 1.912$ Å). The relatively large difference between the 5.48 eV aIE and 5.96 eV vIE of **6** is due to the substantial geometric change after ionization. The aIE is within the experimental range (5.55 ± 0.1 eV).

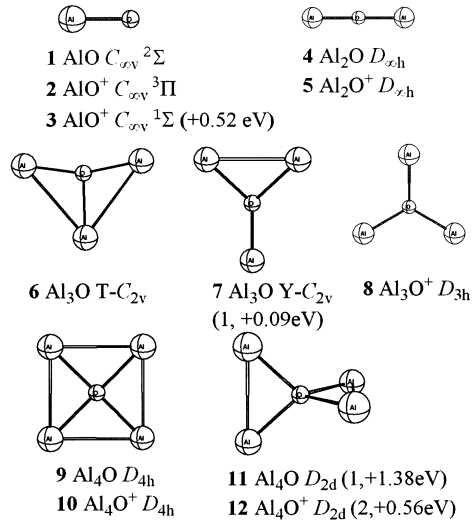

Fig. 4. $AlO^{0,+}$–$Al_4O^{0,+}$ optimized structures. For the higher-lying isomers relative energies and number of imaginary vibrational frequencies (NIMAG) are given in parentheses.

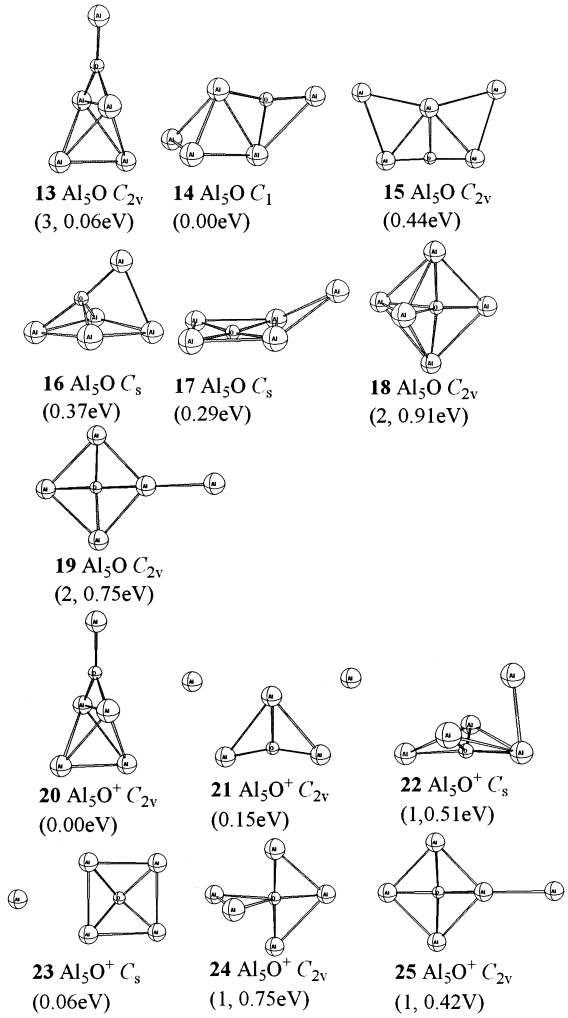

Fig. 5. $Al_5O^{0,+}$ optimized structures. Relative energies and number of imaginary vibrational frequencies (NIMAG) are given in parentheses.

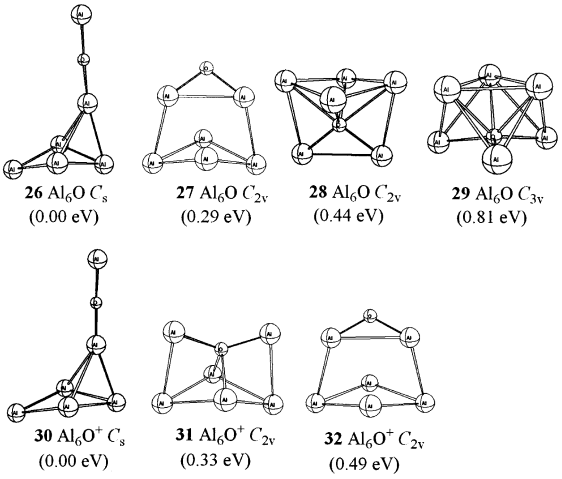

Fig. 6. $Al_6O^{0,+}$ optimized structures. Relative energies are given in parentheses.

Al_4O (**9**) and Al_4O^+ (**10**) both have the square-planar D_{4h} structures computed previously [3,7]. Tetrahedral starting geometries did not converge; the relaxed D_{2d} stationary points, (**11**) neutral and (**12**) cation, have one and two imaginary vibrational frequencies, respectively. The Al−O bond lengths are 1.976 Å (**9**) and 2.036 Å (**10**). The computed aIE (6.36 eV) is in the experimentally determined (5.63−6.43 eV) interval. The vIE (6.73 eV) is somewhat larger.

The most stable neutral Al_5O (**14**) structure (Fig. 5) lacks symmetry (C_1 point group) and was located by further optimization of the C_{2v} structure (**13**) following the vectors of the three imaginary frequencies. This C_{2v} saddle point (**13**) was assigned as the ground state of Al_5O by Yang et al. [7]. Three other local minima are 0.44 eV (**15**), 0.37 eV (**16**) and 0.29 eV (**17**) higher in energy than **14**. Note that **16** was the In_5O global minimum [42]. Adiabatic ionization of **14** (aIE = 5.76 eV) gives **20**, the most stable cation. (The vIE of **14**, 5.97 eV, also lies within the broad 5.63−6.43 eV experimental range). Cation **20** favors C_{2v} symmetry; the other local cation minima are 0.15 eV (**21**) and 0.06 eV (**23**) higher in energy. Optimizations following the imaginary frequencies of each of the three transition states (**22**, **24**, and **25**) lead to the same minimum (**23**).

We located four Al_6O local minima (**26**–**29**, Fig. 6); the most stable form (**26**) has C_s symmetry and is identical to the ground state obtained in reference [7]. The computed vIE values are 6.34 eV (**26**), 6.53 eV (**27**), 6.41 eV (**28**) and 6.39 eV (**29**). While the computed vIE of the most stable Al_6O isomer (**26**) is close to the experimental ∼6.43 eV onset, its aIE (6.15 eV) to the most stable Al_6O^+ cationic structure, **30** (C_s), is not.

4.2 Al_7O and $Al_{15}O$

Al_7O

In startling contrast to the C_{3v} In_7O^+ global minimum with its oxygen inside the cage [42], the lowest energy Al_7O^+ isomer (Fig. 7) has C_{2v} symmetry (**33**), with the oxygen and its "pendant" monovalent Al on the "outside" of the cage. Although favored by In_7O^+, a C_{3v} structure (**34**), was the second best isomer, 0.07 eV higher in energy than **33** at the B3LYP/6-311+G(d) level of theory. A further, extensive isomer search resulted in two local minima, **36** and **38**, but these were 0.64 eV and 0.62 eV, respectively, higher in energy. The most symmetrical D_{5h} structure with a central oxygen atom (**39**) is a saddle point and is more than 1 eV less favorable energetically. The Al_7O^- anion also prefers an exohedral structure, according to a very recent report [18].

Even more peculiar, Al_7O^+ is isoelectronic with the "magic" Al_7N (1.99 eV HOMO-LUMO gap) [48] and Al_7C^- [10,18,49], species both of which, just like In_7O^+, had endohedral C_{3v} global minima resembling **34** [18,48]. However, the C_{2v} isomer (**33**) is energetically more favorable than the C_{3v} Al_7O^+ alternative at both the B3LYP level and CCSD(T) ab initio level (see Tab. 2), though the energy difference is tiny (only 0.03 eV) at the highest theoretical level.

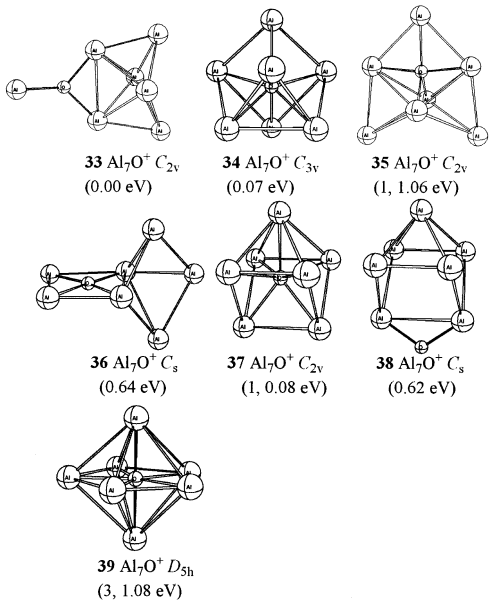

Fig. 7. The B3LYP/6-311+G(d) optimized Al_7O^+ structures. Relative energies and number of imaginary vibrational frequencies (NIMAG) are given in parentheses.

Table 2. The C_{3v} (**32**) vs. C_{2v} (**31**) energy differences (kcal/mol) for the isoelectronic Al_7O^+, Al_7N, Al_7C^- series at the B3LYP and CCSD(T) level.

	B3LYP/ 6-311+G(d)[a]	B3LYP/ 6-311+G(3df)[a]	CCSD(T)/ 6-311+G(d)[b]
Al_7O^+	−1.5	−5.5	−0.8
Al_7N	+12.7	+9.0	+20.8
Al_7C^-	+31.0	+30.3	+45.2

[a] with ZPE corrections;
[b] at B3LYP/6-311+G(3df) optimized geometries.

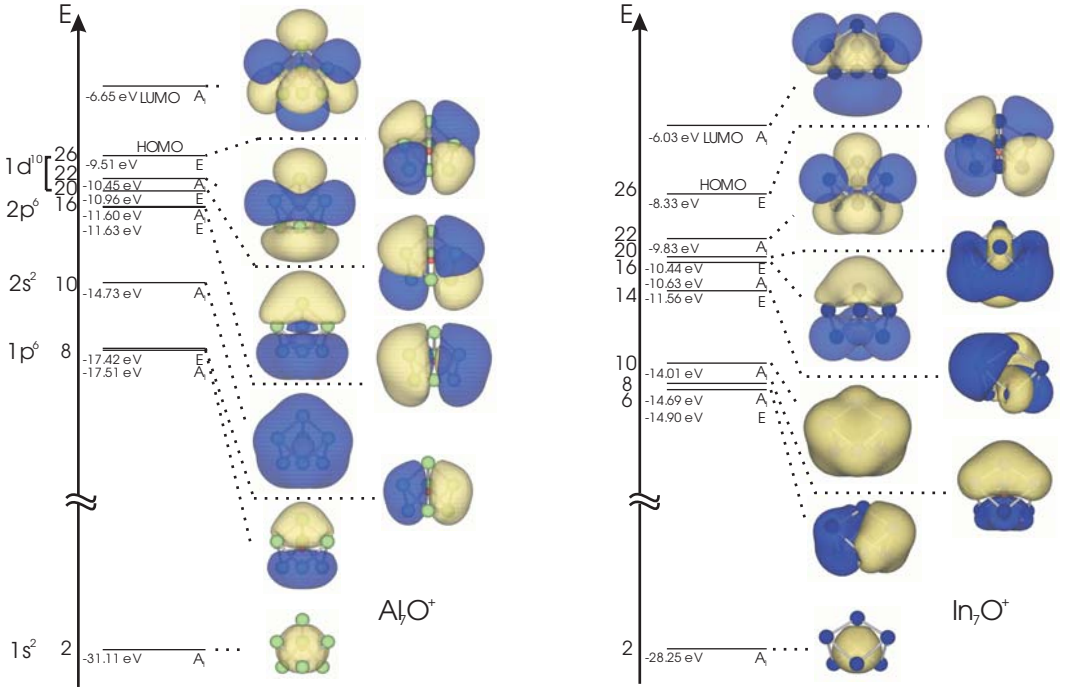

Fig. 8. (Color online) (Left) Energy level sequence and corresponding orbitals for Al_7O^+ (endohedral C_{3v} isomer, **34**) showing 26 electrons in 13 spherical harmonic like orbitals and a large HOMO-LUMO gap, confirming its magic electronic character. (Right) Energy level sequence and corresponding orbitals for In_7O^+.

The IE of Al_7O is lower than the IE's of its neighboring sizes (Al_6O and Al_8O). This is attributable to the closed shell electronic structure of Al_7O^+, and can be rationalized with simple phenomenological shell model considerations. Assuming that oxygen binds two electrons to become the O^{2-} dianion, 19 delocalized electrons remain in Al_7O. After ionization, Al_7O^+ possesses 18 delocalized electrons corresponding to a spherical shell closure ($1s^2/1p^6/1d^{10}$). Alternatively, all the oxygen valence electrons might contribute to a 26 electron total. This is a magic number for (binary) metal clusters doped by an electronegative element ($1s^2/1p^6/2s^2/2p^6/1d^{10}$) [50,51]. An endohedral electronegative atom lowers the energy of s-type (and to a lesser extent p-type) orbitals [52]. Consequently, the relative energy of the $1d^{10}$ shell moves up as is illustrated by the electronic energy level sequences in Figure 8 for the endohedral C_{3v} isomers of Al_7O^+ (low lying minimum) and In_7O^+ (global minimum). Aside from the reduced level degeneracy in the Al_7O^+ C_{2v} isomer (not on figure), the ordering of the energy levels and the shape of the molecular orbitals is not very different from the C_{3v} isomer. The 26 electrons in 13 (spherical harmonic-like) orbitals and the relatively large HOMO-LUMO gaps confirm their "magic number" electronic character.

Albeit small, the energy preference of the highly unusual C_{2v} Al_7O^+ global minimum (**33**) over the usual endohedral C_{3v} structure (**34**) defies a simple rationalization. However, the pronounced trend favoring the C_{2v} isomer with the increasing electronegativity of the doping atom, C<N<O (Tab. 2), provides the clue. The natural charge of oxygen is −1.72 in **33** according to Natural Population analysis; the Al charges are +0.99 on the pendent and +0.57 on the other two adjacent Al's. These four atoms comprise an electrostatically stabilized trigonal OAl_3 moiety, which is bound to the remaining Al_4 unit.

$Al_{15}O$

The ionization energy of $Al_{15}O$ also is relatively low. $Al_{15}O$ has 51 valence electrons; ionization results in the 50 valence electron $Al_{15}O^+$ cation. At first glance, this can be explained by a simple spherical shell model where all electrons are in the outside cage (of a hollow cage structure) [53,54]. However, this is unlikely for $Al_{15}O^+$ due to the shell-crossing (see below) [55,56]. Another model on a 50 electron shell closing can arise in metal clusters from a "crystal field" splitting of the high angular momentum (l) energy levels [19]. This has been suggested to account for the unusually low ionization energy of Al_{17} (51 electrons) [19]. More recently, the unusual stability of the icosahedral $AlPb_{12}^+$ was attributed to a similar shell closing in icosahedral symmetry [55,56]. Most importantly, a shell closing for 50 electrons was predicted computationally using a spherical average pseudopotential method based on DFT to study the electronic and geometric structure of Cs_nO clusters [36,37]. Assuming the oxygen atom at the cluster center, the resulting single electron shell sequence is $1s^2/2s^2/1p^6/3s^2/2p^6/1d^{10}/1f^{14}/4s^2/3p^6$ $(/1g^{18}/2d^{10})$. Notice that the first three shells correspond to the electronic configuration of the central oxygen atom and that there is a 50-electron shell closing in this sequence up to the $3p^6$ shell. Analogously, assuming that the oxygen atom is located in the center of $Al_{15}O^+$, the low ionization energy value observed for $Al_{15}O$ could be related to a 50 electron closed shell structure.

4.3 Al_nO_m, $m > 1$

Distinct features in the IE's also are observed for the more oxygen rich aluminum oxide clusters as function of

their size (Tab. 1 and Supplementary Online Material). For example, the IE's of Al_4O_2, Al_8O_2, and $Al_{16}O_2$ are higher than their neighbors, whereas the IE's of Al_5O_3 and Al_7O_4 are low. The lower IE's of the larger Al_nO_m species with n odd compared to their neighbors with n even are notable: Al_7O_3 to Al_7O_6, Al_9O_5 to Al_9O_7, $Al_{11}O_6$ to $Al_{11}O_9$, $Al_{13}O_8$ to $Al_{13}O_{11}$, and $Al_{15}O_8$ to $Al_{15}O_{12}$ (except for $Al_{15}O_{11}$). The simplest explanation is not linked to electronic shell closing features. Instead, the Al_nO_m species with n = odd are radicals with at least one unpaired electron. This ionizes easily to give electrostatically-stabilized electron paired cations. In contrast, ionization of the paired electron Al_nO_m species results in less favorable radical cations. More sophisticated explanations require quantum chemical calculations but these are beyond the intended scope of this paper.

5 Summary

We produced aluminum oxide clusters in a laser vaporization source. The number of oxygen atoms in the clusters was varied by changing the oxygen content of the He carrier gases. The ionization energies of Al_nO_m species ($n \leq 20$, $m \leq 12$) were bracketed using different ionizing photon energies ranging between 5.37 and 7.89 eV. The structures of singly doped $Al_nO^{+,0}$ (n = 1–5; 7) clusters were deduced using quantum chemical calculations. While a T-shaped C_{2v} structure is favored for Al_3O, the Al_3O^+ cation has a fully symmetric D_{3h} geometry with a closed electronic shell structure. This explains the low IE of Al_3O. The unusual C_{2v} minimum found for Al_7O^+, with the oxygen on the outside of the Al_6 cage and a pendant monovalent Al, is the lowest energy isomer at the B3LYP/6-311+G(3df) level and close in energy with the endohedral C_{3v} alternative, favored by the isoelectronic In_7O^+, Al_7N, and Al_7C^- species. The closed electronic shell structure for Al_7O^+ accounts for the ionization energy of Al_7O being lower than that of the neighboring sizes. Likewise, the IE's for multiply doped Al_nO_m clusters with odd n (and easily ionized unpaired electrons) are lower than their paired electron Al_nO_m neighbors with even n. The low IP of the $Al_{15}O$ radical can be attributed as well to the 50 valence electron closed shell structure of the $Al_{15}O^+$ cation, if oxygen is assumed to be in the center and to contribute all six valence electrons.

The Fund for Scientific Research-Flanders (F.W.O.-Vlaanderen), the Flemish Concerted Action (GOA/2004/02) Research Program, and the Federal Interuniversity Poles of Attraction Program (IAP/V/1) financed the work in Belgium. S.N. and E.J. also thank the F.W.O. for support. National Science Foundation Grant CHE-0716718 funded the project in the USA. Z.C. thanks the Special Coordination Funds for Promoting Science and Technology from the MEXT, Japan, to support his visit at the International Center for Young Scientists, during which this work was finalized. Z.C. also thanks the Research Computing Center of the University of Georgia for providing computational resources.

References

1. S. Desai, H. Wu, C. Rohlfing, L. Wang, J. Chem. Phys. **106**, 1309 (1997)
2. H. Wu, X. Li, X. Wang, C. Ding, L. Wang, J. Chem. Phys. **109**, 449 (1998)
3. A. Boldyrev, P.v.R. Schleyer, J. Am. Chem. Soc. **113**, 9045 (1991)
4. A. Martinez, F. Tenorio, J. Ortiz, J. Phys. Chem. A **105**, 11291 (2001)
5. A. Martinez, L. Sansores, R. Salcedo, F. Tenorio, J. Ortiz, J. Phys. Chem. A **106**, 10630 (2002)
6. A.B.C. Patzer, C. Chang, E. Sedlmayr, D. Sulzle, Eur. Phys. J. D **32**, 329 (2005)
7. P. Yang, J.H. Ge, Z.Y. Jiang, Chin. Phys. **16**, 1014 (2007)
8. T. Ghanty, E. Davidson, J. Phys. Chem. A **103**, 2867 (1999)
9. F.L. King, B.I. Dunlap, D.C. Parent, J. Chem. Phys. **94**, 2578 (1991)
10. B. Leskiw, A.W. Castleman Jr., Chem. Phys. Lett. **316**, 31 (2000)
11. R. Leuchtner, A. Harms, A.W. Castleman Jr., J. Chem. Phys. **91**, 2753 (1989)
12. E.M. Fernández, G. Borstel, J.M. Soler, L.C. Balbas, Eur. Phys. J. D **24**, 245 (2003)
13. E.M. Fernández, L.C. Balbas, G. Borstel, J.M. Soler, Thin Solid Films **428**, 206 (2003)
14. E.M. Fernández, R. Eglitis, G. Borstel, L.C. Balbas, Phys. Stat. Sol. B **242**, 807 (2005)
15. E.M. Fernández, L.C. Balbas, Phys. Stat. Sol. A **203**, 1277 (2006)
16. D. Van Heijnsbergen, K. Demyk, M.A. Duncan, G. Meijer, G. Von Helden, Phys. Chem. Chem. Phys. **5**, 2515 (2003)
17. K. Demyk, D. Van Heijnsbergen, G. Von Helden, G. Meijer, Astron. Astrophys. **420**, 547 (2004)
18. J.U. Reveles, S.N. Khanna, P.J. Roach, A.W. Castleman Jr., Proc. Nat. Acad. Sci. **103**, 18405 (2006)
19. K. Schriver, J. Persson, E. Honea, R. Whetten, Phys. Rev. Lett. **64**, 2539 (1990)
20. M. Pellarin, B. Baguenard, M. Broyer, J. Lermé, J. Vialle, J. Chem. Phys. **98**, 944 (1993)
21. B. Baguenard, M. Pellarin, J. Lermé, J. Vialle, M. Broyer, J. Chem. Phys. **100**, 754 (1993)
22. M. McHenry, M. Eberhardt, R. O'Handley, K. Johnson, Phys. Rev. Lett. **56**, 81 (1986)
23. H. Cheng, R. Berry, R. Whetten, Phys. Rev. B **43**, 10647 (1991)
24. T. Martin, U. Naher, H. Schaber, Chem. Phys. Lett. **199**, 470 (1992)
25. B. Rao, P. Jena, J. Chem. Phys. **111**, 1890 (1999)
26. X. Li, H. Wu, X. Wang, L. Wang, Phys. Rev. Lett. **81**, 1909 (1998)
27. R. Ahlrichs, S. Elliot, Phys. Chem. Chem. Phys. **1**, 13 (1999)
28. M. Pellarin, B. Baguenard, C. Bordas, M. Broyer, J. Lermé, J. Vialle, Z. Phys. D **26**, S137 (1993)
29. B. Baguenard, M. Pellarin, C. Bordas, J. Lermé, J. Vialle, M. Broyer, Chem. Phys. Lett. **205**, 13 (1993)
30. X. Gong, V. Kumar, Phys. Rev. Lett. **70**, 2078 (1993)
31. O. Charkin, D. Charkin, N. Klimenko, A. Mebel, Chem. Phys. Lett. **365**, 494 (2002)
32. P. Lievens, P. Thoen, S. Bouckaert, W. Bouwen, F. Vanhoutte, H. Weidele, R.E. Silverans, A. Navarro-Vázquez, P.v.R. Schleyer, J. Chem. Phys. **110**, 10316 (1999)

33. P. Lievens, P. Thoen, S. Bouckaert, W. Bouwen, F. Vanhoutte, H. Weidele, R.E. Silverans, A. Navarro-Vázquez, P.v.R. Schleyer, Eur. Phys. J. D **9**, 289 (1999)
34. P. Lievens, P. Thoen, S. Bouckaert, W. Bouwen, F. Vanhoutte, H. Weidele, R.E. Silverans, Chem. Phys. Lett. **302**, 571 (1999)
35. H. Limberger, T. Martin, J. Chem. Phys. **90**, 2979 (1989)
36. U. Lammers, A. Mananes, G. Borstel, J.A. Alonso, Solid State Comm. **71**, 591 (1989)
37. U. Lammers, G. Borstel, A. Mananes, J.A. Alonso, Z. Phys. D **17**, 203 (1990)
38. R. Antoine, P. Dugourd, D. Rayane, E. Benichou, M. Broyer, J. Chem. Phys. **107**, 2664 (1997)
39. V. Boutou, M. Lebault, A. Allouche, C. Bordas, F. Paulig, J. Viallon, J. Chevaleyre, Phys. Rev. Lett. **80**, 2817 (1998)
40. V. Boutou, M. Lebault, A. Allouche, C. Bordas, F. Paulig, J. Viallon, J. Chevaleyre, J. Chem. Phys. **112**, 6228 (2000)
41. C. Bréchignac, P. Cahuzac, M. de Frutos, P. Garnier, Z. Phys. D **42**, 303 (1997)
42. E. Janssens, S. Neukermans, F. Vanhoutte, R.E. Silverans, P. Lievens, A. Navarro-Vázquez, P.v.R. Schleyer, J. Chem. Phys. **118**, 5862 (2003)
43. W. Bouwen, P. Thoen, F. Vanhoutte, S. Bouckaert, F. Despa, H. Weidele, R.E. Silverans, P. Lievens, Rev. Sci. Instr. **71**, 54 (2000)
44. A. McLean, G. Chandler, J. Chem. Phys. **72**, 5639 (1980)
45. G. Petersson, M. Allaham, J. Chem. Phys. **94**, 6081 (1991)
46. A. Becke, J. Chem. Phys. **98**, 5648 (1993)
47. *Gaussian 03*, M.J. Frisch, G.W. Trucks, H.B. Schlegel, G.E. Scuseria, M.A. Robb, J.R. Cheeseman, J.A. Montgomery Jr, T. Vreven, K.N. Kudin, J.C. Burant, J.M. Millam, S.S. Iyengar, J. Tomasi, V. Barone, B. Mennucci, M. Cossi, G. Scalmani, N. Rega, G.A. Petersson, H. Nakatsuji, M. Hada, M. Ehara, K. Toyota, R. Fukuda, J. Hasegawa, M. Ishida, T. Nakajima, Y. Honda, O. Kitao, H. Nakai, M. Klene, X. Li, J.E. Knox, H.P. Hratchian, J.B. Cross, V. Bakken, C. Adamo, J. Jaramillo, R. Gomperts, R.E. Stratmann, O. Yazyev, A.J. Austin, R. Cammi, C. Pomelli, J.W. Ochterski, P.Y. Ayala, K. Morokuma, G.A. Voth, P. Salvador, J.J. Dannenberg, V.G. Zakrzewski, S. Dapprich, A.D. Daniels, M.C. Strain, O. Farkas, D.K. Malick, A.D. Rabuck, K. Raghavachari, J.B. Foresman, J.V. Ortiz, Q. Cui, A.G. Baboul, S. Clifford, J. Cioslowski, B.B. Stefanov, G. Liu, A. Liashenko, P. Piskorz, I. Komaromi, R.L. Martin, D.J. Fox, T. Keith, M.A. Al-Laham, C.Y. Peng, A. Nanayakkara, M. Challacombe, P.M.W. Gill, B. Johnson, W. Chen, M.W. Wong, C. Gonzalez, J.A. Pople, Gaussian, Inc., Wallingford CT, 2004
48. Q. Sun, Q. Wang, X. Gong, V. Kumar, Y. Kawazoe, Eur. Phys. J. D **18**, 77 (2002)
49. H. Kawamata, Y. Negishi, A. Nakajima, K. Kaya, Chem. Phys. Lett. **337**, 255 (2001)
50. C. Yeretzian, J. Phys. Chem. **99**, 123 (1995)
51. C. Yannouleas, P. Jena, S. Khanna, Phys. Rev. B **46**, 9751 (1992)
52. E. Janssens, S. Neukermans, P. Lievens, Curr. Opin. Solid State Mater. Sci. **8**, 185 (2004)
53. A. Hirsch, Z. Chen, H. Jiao, Angew. Chem. Int. Ed. **39**, 3915 (2000)
54. Z. Chen, H. Jiao, A. Hirsch in *Fullerenes: From Synthesis to Optoelectronic Applications*, edited by D.M. Guldi, N. Martin (Kluwer Academic Publishers, Dortrecht, The Netherlands, 2002)
55. Z. Chen, S. Neukermans, X. Wang, E. Janssens, Z. Zhou, R.E. Silverans, R.B. King, P.v.R. Schleyer, P. Lievens, J. Am. Chem. Soc. **128**, 12829 (2006)
56. S. Neukermans, E. Janssens, Z. Chen, R.E. Silverans, P.v.R. Schleyer, P. Lievens, Phys. Rev. Lett. **92**, 163401 (2004)